crystals

MDPI

Article

Preparation of Ti-Doped ZnO/Bi_2O_3 Nanofilm Heterojunction and Analysis of Microstructure and Photoelectric Properties

Zhenying Chen [1,*], Xiuqing Cao [2], Yuyang Huang [3], Shuang Zhang [1], Wenjian Pan [1] and Wen Deng [3]

[1] College of Science, Beibu Gulf University, Qinzhou 535011, China
[2] College of Electronic Information, Guangxi Minzu University, Nanning 530006, China
[3] College of Physical Science and Engineering, Guangxi University, Nanning 530004, China
* Correspondence: czy1@bbgu.edu.cn

Abstract: Ti-doped ZnO (TZO) and Bi_2O_3 thin films were designed and deposited by magnetron sputtering successively on ITO glass substrate to form a Ti-doped ZnO/Bi_2O_3 (TZO/Bi_2O_3) heterojunction. Microstructure and photoelectric properties of TZO, Bi_2O_3, and TZO/Bi_2O_3 films were tested and characterized. The results showed that TZO film with a hexagonal wurtzite structure was preferentially grown along the crystal plane (002), had a good crystallization state, and was an N-type semiconductor film with high transmittance (90%) and low resistivity (4.68×10^{-3} Ω·cm). However, the Bi_2O_3 film sputtered in an oxygen-containing atmosphere and was a polycrystalline film that was preferentially grown along the crystal plane (111). It had a lower crystallization quality than TZO film and was a P-type semiconductor film with low transmittance (68%) and high resistance (1.71×10^2 Ω·cm). The I–V curve of TZO/Bi_2O_3 composite films showed that it had an obvious heterojunction rectification effect, which indicates that the PN heterojunction successfully formed in TZO/Bi_2O_3 films.

Keywords: TZO film; Bi_2O_3 film; TZO/Bi_2O_3 heterojunction; magnetron sputtering; optoelectronic properties

check for updates

Citation: Chen, Z.; Cao, X.; Huang, Y.; Zhang, S.; Pan, W.; Deng, W. Preparation of Ti-Doped ZnO/Bi_2O_3 Nanofilm Heterojunction and Analysis of Microstructure and Photoelectric Properties. *Crystals* **2023**, *13*, 264. https://doi.org/10.3390/cryst13020264

Academic Editor: Andreas Thissen

Received: 11 December 2022
Revised: 28 January 2023
Accepted: 30 January 2023
Published: 2 February 2023

Copyright: © 2023 by the authors. Licensee MDPI, Basel, Switzerland. This article is an open access article distributed under the terms and conditions of the Creative Commons Attribution (CC BY) license (https://creativecommons.org/licenses/by/4.0/).

1. Introduction

With improvements in the integration and miniaturization of electronic devices, there is a growing demand for miniature low-voltage varistors that protect integrated circuits. The resistance value of the varistor is a nonlinear relationship with the voltage at both ends. ZnO-based varistor is a ceramic electronic device with excellent performance which is sintered with ZnO as the main raw material by adding various trace metal oxides, such as Bi_2O_3 and TiO_2 [1–3]. The additive Bi_2O_3 mainly separates ZnO grains to form a thin layer of bismuth-rich grain boundary. Thus, the grain boundaries of Bi_2O_3 and its adjacent ZnO grains form a pair of back-to-back heterojunctions. Many of these heterojunction units are intricately connected in series and parallel, which forms the microstructure of the ZnO varistor [4,5]. Many back-to-back heterojunctions in a series will lead to high voltage varistors. Therefore, it is difficult to achieve low voltage ZnO-based varistor in ceramic bulk materials. Meanwhile, such a complex microstructure makes it difficult to study the conduction mechanism of the varistor. At present, there is no ideal theoretical model that satisfactorily explains its conduction mechanism. Therefore, by reducing the number of back-to-back heterostructures in the materials as much as possible, we can realize low voltage ZnO varistor and effectively study its conductive mechanism of varistor. Thin film materials can reduce the number of heterojunctions, enabling the creation of low voltage ZnO-based varistors.

The key problem in successfully preparing low voltage ZnO varistor film is whether there is a heterojunction effect between the ZnO film and the Bi_2O_3 film. However, there are few reports on the heterojunction effect between Bi_2O_3 and ZnO films. For example,

anoxic zinc oxide ($ZnO_{0.81}$) film was prepared using the magnetron sputtering method, and then the zinc oxide film was hot dipped into Bi_2O_3 powder. The relationships between its performance and the hot-dipping temperature and hot-dipping time were studied. The sample fabricated by hot-dipping in Bi_2O_3 at 400 °C for 40 min had the highest α (15.1) and V_B (0.0176 V/nm) and the lowest I_L (0.0223 mA/cm^2) [6,7]. However, most Bi_2O_3 permeated into the film and deposited among ZnO grains to form many grain boundary phases during the hot-dipping process. Its structure is still complex, and it is difficult to explore the micro-mechanism of heterojunction between a single ZnO grain and the grain boundary containing Bi_2O_3. In addition, a few other studies on ZnO/Bi_2O_3 heterojunctions focus on the direct application of photocatalysis and light absorption, but the physical nature of the heterojunctions is less explored, and ZnO/Bi_2O_3 preparation methods are relatively complex [8,9]. Therefore, composite ZnO/Bi_2O_3 films similar to the heterojunction unit in ZnO varistor ceramics are expected to be designed and prepared using simple methods for further research and development of low voltage ZnO varistors.

Magnetron sputtering methods have advantages of a strong bonding force, compactness, uniformity, and mature industrialization conditions [10,11]. In addition, the columnar ZnO film prepared by magnetron sputtering exhibits preferential orientation growth which can ensure that a single grain grows in the film thickness direction [12]. If the ZnO film is coated with Bi_2O_3 film, a single heterojunction similar to the heterojunction unit in ZnO varistor ceramics can be synthesized. Based on this, the ZnO and Bi_2O_3 thin films mentioned in this paper were prepared using magnetron sputtering.

It is well known that the general method is to increase the resistance of the grain boundary (Bi_2O_3) and decrease the grain (ZnO) resistance in order to enhance the performance of a varistor. Accordingly, the conductivity of ZnO films should be increased, while that of Bi_2O_3 films should be reduced. However, the intrinsic ZnO film has high resistivity at room temperature, and an N-type semiconductor with good conductivity can be formed by ordinary doping. For example, introducing trace amounts of Al, Ga, Ta, and Mg into ZnO film can effectively improve film conductivity [13–16]. Among all ZnO doping studies, aluminum doping is the most in-depth and extensive. For titanium doping, the ionic radius of Ti^{4+} (0.068 nm) is smaller than that of Zn^{2+} (0.074 nm). Ti^{4+} can easily enter the ZnO lattice to replace Zn^{2+}, and Ti^{4+} ions with higher valence than Zn^{2+} can provide more free electrons. This would increase carrier concentration and decrease resistivity [17,18]. Based on the above analysis, and with reference to the fact that trace TiO_2 is often added to the raw materials of the ZnO-based varistor, N-type titanium doped ZnO films (TZO) were obtained by magnetron sputtering using a TiO_2-doped ZnO target.

As for Bi_2O_3 film, due to the large difference in element electronegativity between Bi atoms and O atoms, the proportion of ionic bonds in chemical bonds is relatively large, and atoms can easily break away from ionic bonds. There is a large concentration of point defects in the film, and the atomic ratio of bismuth to oxygen in the film usually deviates from that in standard Bi_2O_3. If there are more bismuth atom vacancies in the film, the acceptor-type energy level can be easily formed, resulting in increased hole concentration and P-type semiconductor conductivity. This has been reported in the literature [19]. In order to ensure that the Bi_2O_3 film prepared by magnetron sputtering is a P-type semiconductor, a small amount of oxygen was introduced when sputtering the Bi_2O_3 film in this experiment to create an oxygen-rich film growth atmosphere so that the Bi atoms in the film had a high vacancy concentration, with the carrier hole playing a dominant role. In addition, considering that only a trace amount of Bi_2O_3 was doped to the raw materials of ZnO-based varistor, when preparing Bi_2O_3 films in this experiment, the coating time was correspondingly controlled to be lower than that of the TZO film; therefore, the Bi_2O_3 films had a smaller thickness than TZO films.

In this research, TZO film and Bi_2O_3 film were prepared according to the above design, and then TZO film and Bi_2O_3 film were compounded into a heterojunction. The microstructures and photoelectrical properties of all the samples were tested, and their

physical mechanisms were analyzed, which laid a foundation for further study of varistors mechanisms and the development of a ZnO-based low voltage film varistor.

2. Experiment

2.1. Target Material Preparation

TZO target material: TiO_2 powder with 99.99% purity (Shanghai Aladdin Biological Reagent Co., Ltd., Shanghai, China) and ZnO powder with 99.99% purity (Tianjin Guangfu Chemical Reagent Co., Ltd., Tianjin, China) were selected as raw materials. The mass ratio of the two powders was ZnO:TiO_2 = 98%:2%. The material was mixed evenly with ultrapure water as the solvent and then dried using a ball mill. The dried mixed powder was pressed into a green body using a powder press. The green body was sintered at 1450 °C in a muffle furnace to form a TZO ceramic target material with a diameter of about 60 mm and a thickness of about 3 mm.

Bi_2O_3 target material: Bi_2O_3 powder with 99.99% purity (Shanghai Aladdin Biological Reagent Co., Ltd., Shanghai, China) was used as the raw material, and the green body was made by drying, granulating, and pressing. The green body was sintered at 750 °C and kept warm for 8 h to produce Bi_2O_3 target material with a diameter of about 59 mm and a thickness of about 3 mm. Considering that the bismuth oxide target material would easily crack during sputtering, the bismuth oxide target was bound to an oxygen-free copper plate of the same size, with a thickness of 1.5 mm.

2.2. Preparation of the TZO/Bi_2O_3 Films

The substrates of the TZO/Bi_2O_3 films were ITO conductive glass (Hefei Kejing Material Technology Co., Ltd., Hefei, China). The thickness of the ITO film deposited on the glass surface was 135 nm, and the resistivity was less than 15 Ω/sq. The ITO glass was ultrasonically cleaned in absolute ethanol and ultrapure water for 10 min successively, and then it was blown dry using high purity nitrogen and finally placed in a vacuum drying oven at 80 °C.

The structure design of the heterojunction is shown in Figure 1. TZO/Bi_2O_3 composite films were prepared using a magnetron sputtering instrument (JGP-450A, Chinese Academy of Sciences Co., Ltd., Beijing, China) to continuously sputter TZO thin films and Bi_2O_3 thin films on clean ITO substrates through RF magnetron sputtering. During the sputtering process, the target-base distance was set to 60 mm, the substrate temperature was 150 °C, the background vacuum was 2.0×10^{-4} Pa, and the target pre-sputtering time was 30 min. Other process parameters are listed in Table 1.

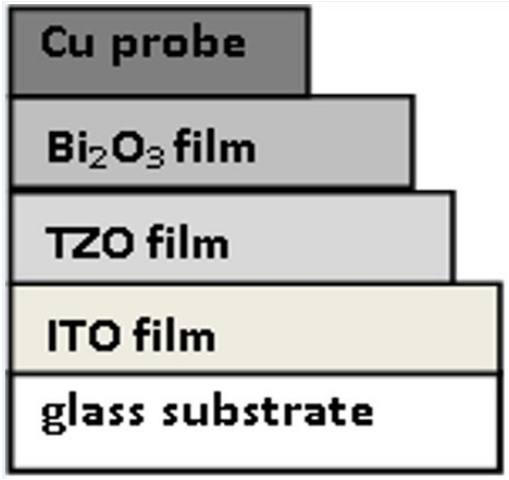


Figure 1. Schematics of TZO/Bi_2O_3 film.

Table 1. Sputtering process parameters of TZO/Bi_2O_3 film.

Name of the Film	Sputtering Pressure (Pa)	Argon Flow (sccm)	Oxygen Flow (sccm)	Sputtering Power (W)	Sputtering Time (min)
TZO	0.5	35	0	150	50
Bi_2O_3	0.6	50	0.5	75	20

2.3. Characterization of TZO/Bi_2O_3 Films

DektakXT probe-type surface profiler (BRUKER, Billerica, MA, USA) was used to test film thickness. A field emission electron microscope (Hitachi SU8020, Tokyo, Japan) was used to test the microscopic surface morphology. The mean size of the zinc oxide grains in the film samples was evaluated using Nano-Measurer (version 1.2) software and the SEM images were obtained. The cross-sectional morphology of the TZO/Bi_2O_3 thin film heterojunction was analyzed using a Field Emission Scanning Electron Microscope (360 Zeiss Gemini, Aalen, Germany), and a DX-2700A X-ray diffractometer (CuKα_1 target, wavelength 0.15406 nm, Dandong HAOYUAN Instrument Co., Ltd., Dandong, China) was used to test its microstructure and growth orientation. A hall tester (8800, Swin, Taiwan, China) was used to measure room temperature resistivity, carrier type, concentration, and mobility. Transmittance was measured using an ultraviolet-visible spectrophotometer (UV-2700, Shimadzu, Kyoto, Japan). The digital source meter (B2901A, Agilent, Santa Clara, CA, USA) was used to characterize the I–V characteristics of heterojunction films.

3. Experimental Results and Discussion

3.1. Appearance of TZO/Bi_2O_3 Films

The structure of the TZO/Bi_2O_3 heterojunction film is shown in Figure 1. ITO was the bottom electrode which was sequentially plated with TZO film and Bi_2O_3 film. A Cu electrode formed by pressing a pure oxygen-free copper probe on the film surface during electrical performance testing. The film thickness was characterized by the average value of the profilometer test data for the same sample at different positions, and the film thickness of each layer is shown in Table 2. The TZO coating time was 50 min, the film thickness was 522.1 nm, and the average growth rate was 10.4 nm/min. The average growth rate of the Bi_2O_3 film was 10.2 nm/min. The two films in heterojunctions had a similar growth rate.

Table 2. The thickness of each layer of TZO/Bi_2O_3 heterojunction film.

Name of the Film	TZO	Bi_2O_3	TZO/Bi_2O_3
Film thickness (nm)	522.1	203.5	725.6

3.2. Micromorphology of TZO/Bi_2O_3 Films

Figure 2 shows Scanning Electron Microscope (SEM) images for the TZO and Bi_2O_3 films. The TZO and Bi_2O_3 films belonged to the same TZO/Bi_2O_3 heterojunction. It can be seen from Figure 2 that the TZO thin film sample prepared by magnetron sputtering had uniform and dense grains, a long worm-like shape, and a smooth surface. In Bi_2O_3 thin film samples sputtered in an oxygen atmosphere, the grains were spherical and had a relatively uniform grain size, but their distribution was relatively sparse. Comparing the SEM of the TZO film with the Bi_2O_3 film, it can also be seen that the surface of TZO film had a smaller grain boundary width, smaller cavity size, and better crystal state. In general, the crystalline state of the TZO film is better than that of the Bi_2O_3 film. This is mainly because Bi_2O_3 has a low melting point of 824 °C, which leads to a lower target sintering temperature. Therefore, the target material structure is not dense enough. Excessively high sputtering power can easily crack the target and result in a relatively low sputtering power of the Bi_2O_3 film. Since there are few target particles sputtered per unit of time, the deposited thin film grains are relatively loose. The mean size of the zinc oxide grains in the samples was evaluated using Nano-Measurer 1.2 software from the obtained SEM images.

According to software statistics, TZO grains were wormlike, with an average width of 30 nm and an average length of 70 nm. Bi_2O_3 grain was round, with an average diameter of 40 nm. The grain shapes of these two films are consistent with those reported in the relevant literature [18,20].

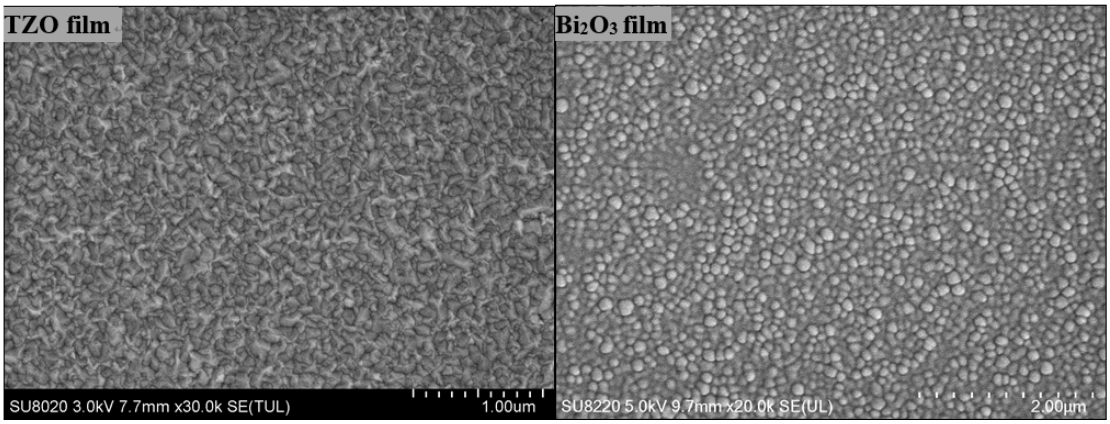


Figure 2. SEM micrographs of TZO and Bi_2O_3 films.

A cross-sectional SEM image of the TZO/Bi_2O_3 composite films is shown in Figure 3. The TZO (~540 nm) and Bi_2O_3 (~220 nm) films were sequentially deposited on the ITO glass substrate. Bi_2O_3 did not penetrate the TZO film completely, and there was an obvious interface between the two layers. The thicknesses of the TZO and Bi_2O_3 films obtained by SEM testing were similar to those obtained using a profilometer, as shown in Table 2. It can also be seen that TZO films grew in the columnar morphology, which is well known for ZnO film deposition on glass substrates [12,21].

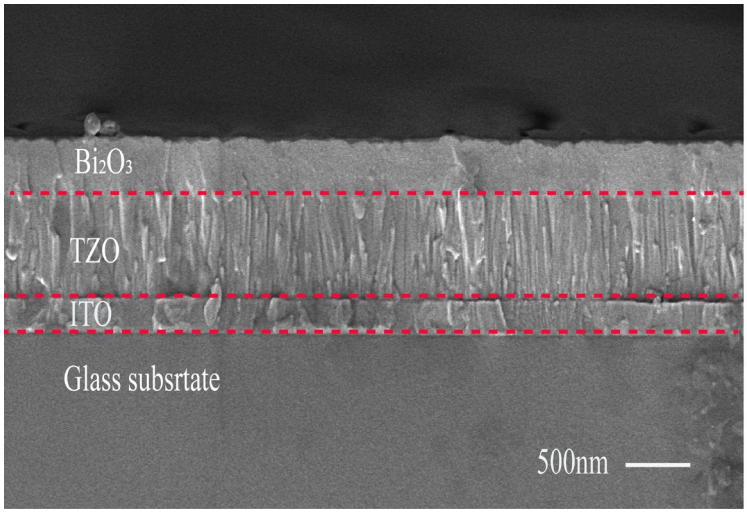


Figure 3. A cross-sectional SEM image of TZO/Bi_2O_3 thin film heterojunction.

3.3. Microstructure of TZO/Bi_2O_3 Films

Figure 4 shows the XRD spectral lines of all thin samples. As can be seen from the figure, the XRD spectrum of the TZO film had a strong diffraction peak around 34.4°, which corresponded to the inherent diffraction peak of the ZnO (002) crystal plane, indicating that the film is a polycrystalline film with a hexagonal wurtzite structure, good C-axis preferred orientation, good crystallinity, and high purity. Neither TiO_2 nor Zn_2TiO_4 second phase was observed in the scanning range of 20–80° (2θ). This implies that titanium atoms may replace zinc atomic sites substitutionally or incorporate them interstitially in the hexagonal lattices. The XRD spectra of the TZO film are consistent with the results reported in the

literature [22–24]. For the XRD of the Bi_2O_3 film sputtered in an oxygen atmosphere, there was a prominent main peak line around 2θ = 27.7°. This strong diffraction peak can be attributed to the crystal plane (111) of the intrinsic Bi_2O_3 film, which indicates that the film exhibits an obvious preferential growth trend along the crystal plane (111). It suggests that this crystal plane is a tight plane with a small crystal plane spacing. It can also be seen that the composition of the TZO/Bi_2O_3 film did not change after the combination of TZO and Bi_2O_3. The XRD spectra of Bi_2O_3 film are also consistent with the results reported in the literature [25].

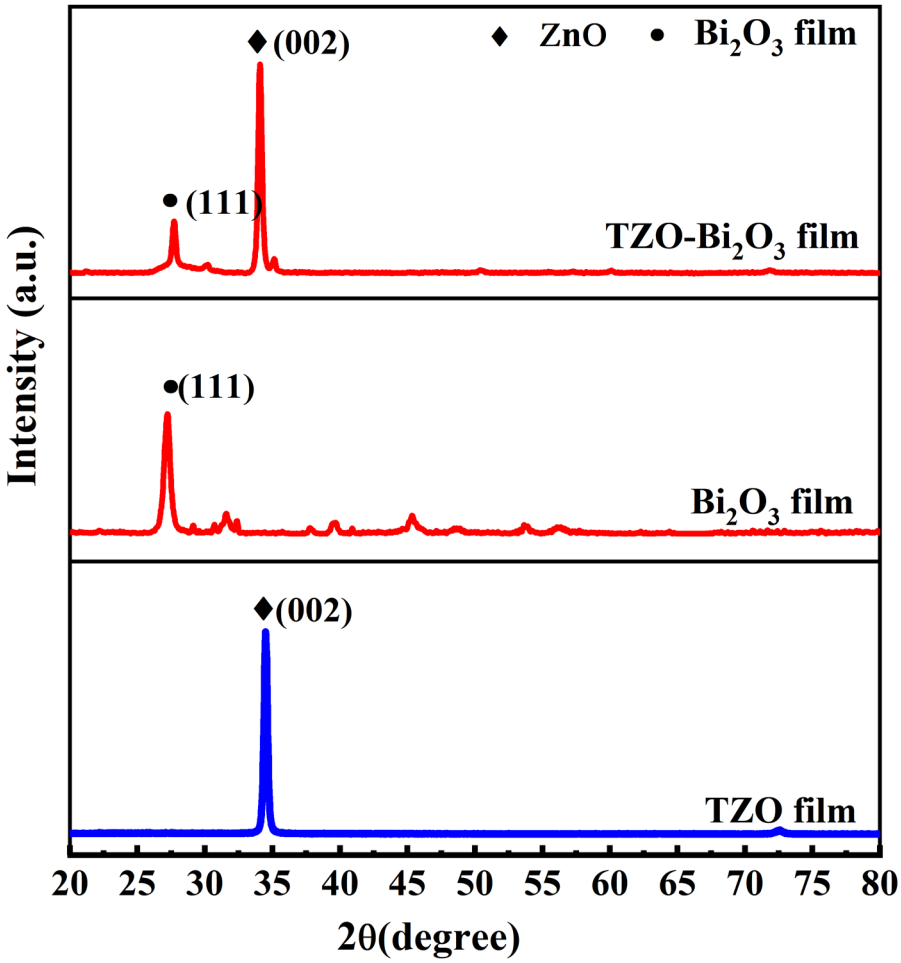


Figure 4. XRD analysis for each layer of TZO/Bi_2O_3 heterojunction film.

The XRD diffraction peak positions (2θ), FWHM, and grain sizes were calculated using the Scherrer formula and are shown in Table 3. As can be seen from Table 3, compared with the standard intrinsic diffraction peaks of ZnO (PDF36-1451) and Bi_2O_3 (PDF16-0654), the 2θ of TZO and Bi_2O_3 prepared in this study were larger. For Ti-doped TZO films, lattice distortion was caused by the small radius of Ti atoms entering the ZnO lattice to replace the Zn atoms. For Bi_2O_3 films prepared in an oxygen-rich atmosphere, oxygen atoms with a radius smaller than the bismuth atoms entering the film may replace the position of the bismuth atoms and also cause lattice distortion, both of which will make the lattice constant smaller, thereby causing the diffraction peak position to shift to a larger angle. According to the Scherrer formula, the grain size of ZnO perpendicular to the film surface was about 28 nm, while the grain size of Bi_2O_3 perpendicular to the film surface was about 26 nm.

Table 3. Parameters of XRD diffraction peaks and grain sizes of TZO and Bi_2O_3 films.

Name of the Film	2θ(°)	2θ of Intrinsic Oxide (°)	FWHM (°)	Grain Size (nm)
TZO	34.481	34.421	0.298	28.197
Bi_2O_3	27.756	27.249	0.320	25.996

3.4. Optical Properties of the TZO/Bi_2O_3 Films

The transmittance curves of the TZO film, Bi_2O_3 film, and TZO/Bi_2O_3 films in the 300 nm–850 nm wavelength range are shown in Figure 5. The average transmittance of these samples in the visible light range (380–780 nm) is shown in Table 4. As can be seen from Figure 5 and Table 4, single-layer TZO had a relatively high transmittance of 90%. In addition, the transmittance curve dropped sharply around 360 nm, which appears to be the intrinsic absorption edge. The photon energy was 360 nm, which was slightly higher than the intrinsic bandgap width of ZnO (3.37 eV). When the incident photon energy exceeds the photon energy at 360 nm, the film will absorb the photon energy to excite electrons in the valence band to the conduction band, resulting in a sharp decrease in transmittance. The Bi_2O_3 film had a slightly lower transmittance of 68% in the visible light region, and its transmittance curve underwent a sharp drop around 400 nm, showing absorption edge. The photon energy corresponding to this wavelength was also slightly higher than the forbidden band width of the intrinsic Bi_2O_3. The figure shows that Bi_2O_3 film had a narrower optical band gap than TZO. Table 4 shows that the heterojunction film had an average transmittance of 65% in the visible light region, showing a certain degree of transparency.

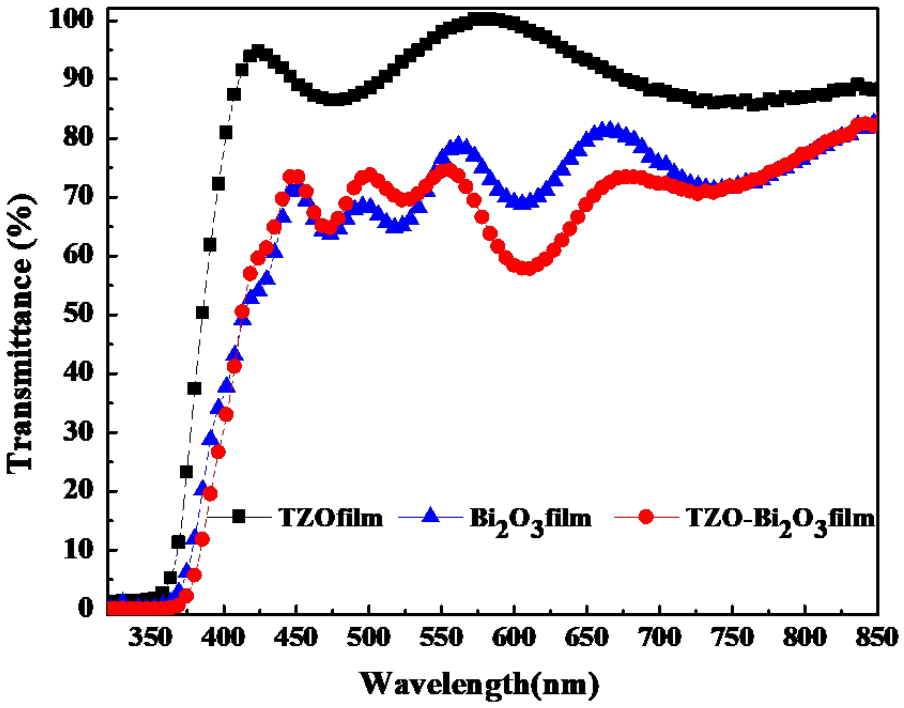


Figure 5. Optical transmittance spectra of each layer of TZO/Bi_2O_3 heterojunction film.

Table 4. Average optical transmittances of each layer of TZO/Bi_2O_3 heterojunction film (380–780 nm).

Name of the Film	TZO Film	Bi_2O_3 Film	TZO/Bi_2O_3 Film
Average transmittance (%)	90	68	65

The optical bandgap (E_g) of ZnO and Bi_2O_3 films can be determined by their optical transmittance spectra, as shown in Figure 5. To obtain the E_g value, the optical absorption coefficient (α) of the film is first estimated according to the following formula:

$$\alpha = -\frac{\ln T}{d} \quad (1)$$

where T is the optical transmittance of the films and d is the thickness of the films. ZnO and Bi_2O_3 are generally considered direct bandgap materials, so E_g can be determined using Tauc's formula:

$$\alpha h\upsilon = C\left(h\upsilon - E_g\right)^{\frac{1}{2}} \quad (2)$$

where C is a constant, h is Planck's constant, υ is the frequency of light, and $h\upsilon$ is the photon energy of incident light. The E_g value is obtained by plotting $(\alpha h\upsilon)^2$ versus $h\upsilon$ and then extrapolating the linear part of the curve to the horizontal axis [22,26,27]. The $(\alpha h\upsilon)^2$~$h\upsilon$ curves and E_g values for the TZO and Bi_2O_3 films are shown in Figure 6. The TZO film had a forbidden band width of 3.47 eV, while Bi_2O_3 had a slightly lower optical band gap (3.10 eV) than the TZO film, which is close to the reported literature [17,28]. The optical band gaps in these two films are larger than the forbidden band width of intrinsic semiconductors. For the TZO film, the doping concentration was up to 2% due to the large difference in electron configuration (Ti:$3d^2 4s^2$, Zn:$3d^{10} 4s^2$). Ti atoms replace zinc sites in the ZnO lattice and will result in additional weakly bound electrons. Once the impurity band generated by these weakly bound electrons becomes wide enough to reach the edge of the conducting band, the effective ionization energy of these shallow donors will disappear and lead to an increase in carrier concentration. Too many carriers will fill up the lowest energy level in the conduction band and cause the so-called Burstein–Moss shift effect. That is, the Fermi level enters the conduction band, and the absorption edge of the intrinsic light is blue shifted; therefore, the optical band gap widens [22,24]. For Bi_2O_3 film, the band gap became wider, which may be due to the increase in effective mass caused by oxygen atoms or its poor crystal quality.

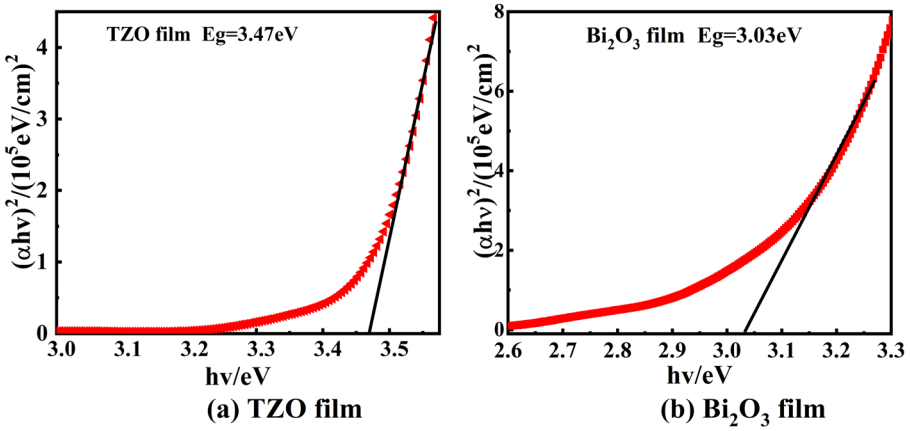


Figure 6. Plots of $(\alpha h\upsilon)^2$ versus photon energy ($h\upsilon$) of (**a**) TZO and (**b**) Bi_2O_3 films.

3.5. Electrical Properties of the TZO/Bi_2O_3 Films

The resistivity, carrier concentration, and mobility of the films were measured at room temperature using a Hall tester. The electrical performance parameters are shown in Table 5. It can be seen from the table that the TZO thin film sample had a relatively high carrier concentration of up to 1.17×10^{20} cm^{-3} and a mobility of 11.40 $cm^2 \cdot v^{-1} \cdot s^{-1}$, and it belonged to the N-type semiconductor. The electrical resistivity of the TZO film was as low as 4.68×10^{-3} Ω·cm, which is close to that of the same films reported in the literature [17]. After Ti^{4+} ion replaced Zn^{2+}, two additional carriers were provided. Ti^{4+} ion also had a doping ratio of up to 2%, which can provide many free electrons. In addition, the film

was uniform, dense, and flat, and it had a good crystalline state; therefore, the capture and scattering of the carriers was weak, which further increased carrier concentration and carrier mobility. It is because of such a high carrier concentration that the Burstein–Moss shift effect was produced, which is consistent with the above analysis of E_g widening. As for the Bi_2O_3 film prepared in the oxygen-rich sputtering atmosphere, there were more vacancies in Bismuth atoms, which formed an acceptor-type energy level in hole provision. It belonged to the P-type semiconductor and had a relatively high resistivity of up to 1.71×10^2 Ω·cm, a relatively small carrier concentration of 3.89×10^{15} cm^{-3}, and a mobility of 9.40 $cm^2 \cdot v^{-1} \cdot s^{-1}$. The grain arrangement of Bi_2O_3 film was loose, the grain boundary between the grains was relatively wide, and the hole between the grains was relatively large, so the crystal state of the film was not good, resulting in large scattering of carriers and a small carrier mobility.

Table 5. Hall effect measurements for TZO and Bi_2O_3 films.

Name of the Film	Electrical Resistivity (Ω·cm)	Carrier Concentration (cm^{-3})	Carrier Mobility ($cm^2 \cdot v^{-1} \cdot s^{-1}$)	Conductivity Type
TZO film	4.68×10^{-3}	1.17×10^{20}	11.40	N-type
Bi_2O_3 film	1.71×10^2	3.89×10^{15}	9.40	P-type

The I–V characteristics of the TZO/Bi_2O_3 film heterojunction were tested and characterized by a digital source meter (model B2901A). Due to the complex structure of the composite film and the inconsistent Fermi energy between the adjacent film layers, which would determine whether there was a heterojunction effect between the TZO and Bi_2O_3 films, the I–V characteristic curves between the adjacent film layers were sequentially tested in this study. The results are shown in Figure 7. The I–V curves between other adjacent films were straight, except for the ITO and Bi_2O_3 films, which indicates that they were in an ohmic contact state without the unique nonlinear effect of P-N junction. However, the I–V curves between TZO and Bi_2O_3 films clearly exhibited a heterojunction rectification effect. The junction exhibited a threshold voltage (V_{TH}) of 1.04 V. In short, the heterojunction was successfully synthesized between the TZO and Bi_2O_3 films. This heterojunction formed by the TZO and Bi_2O_3 films prepared by magnetron sputtering is rarely reported [26].

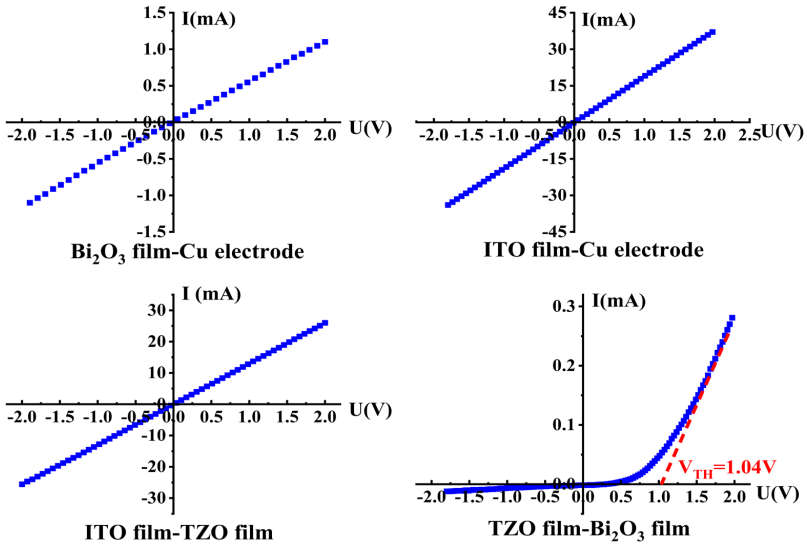


Figure 7. I–V measurement curve of adjacent layer of TZO/Bi_2O_3 heterojunction film.

4. Conclusions

TZO film, Bi_2O_3 film, and TZO/Bi_2O_3 composite film were designed and prepared by magnetron sputtering according to the microstructure of ZnO varistor. Microstructure and photoelectric properties of TZO, Bi_2O_3, and TZO/Bi_2O_3 films were tested and characterized.

The results showed that TZO film was a polycrystalline nanofilm preferentially grown along the crystal plane (002), and the grain size along the normal direction of the crystal plane was about 28 nm. Its surface was dense and its grain shape was worm-like, with an average width of 30 nm and an average length of 70 nm. It had a forbidden band width of 3.47 eV. It was an N-type semiconductor film with high transmittance (90%) in the visible light region and low resistivity (4.68×10^{-3} Ω·cm). However, the Bi_2O_3 film sputtered in an oxygen-containing atmosphere was a polycrystalline film preferentially grown along the crystal plane (111), and its grain size along the normal direction of the crystal plane was about 26 nm. Its grains were loose, and its grain shape was round, with an average diameter of 40 nm. It had a slightly lower optical band gap (3.10 eV) than that of the TZO film, and it was a P-type semiconductor film with low transmittance (68%) in the visible light region and high resistance (1.71×10^2 Ω·cm). The I–V curve of the TZO/Bi_2O_3 composite films showed an obvious heterojunction rectification effect, which indicates that the P-N heterojunction was successfully formed in the TZO/Bi2O3 films, with a transmittance of 65% in the visible light region. The junction exhibited a threshold voltage (V_{TH}) of 1.04 V. TZO/Bi_2O_3 films may be suitable for use as ZnO-based low voltage varistors and solar cells in the future. This work also lays the foundation for further research and development of ZnO low voltage varistors.

Author Contributions: Z.C., S.Z. and W.D. conceived and designed the experiments. Z.C., X.C., Y.H. and W.P. performed the experiments. Z.C., X.C. wrote the paper. All authors discussed and analyzed the results. All authors have read and agreed to the published version of the manuscript.

Funding: This research was funded by the National Natural Science Foundation of China (NSFC) (Grant No. 51862031) and the Doctoral Scientific Research Staring Foundation of Beibu Gulf University in China (Grant No. 18KYQD50).

Data Availability Statement: Data is contained within the article.

Conflicts of Interest: The authors declare no conflict of interest.

References

1. Shi, M.; Liu, J.; Li, J.; Xu, J.; Jiang, M.; Xu, D. Effects of the electric field on microstructure and electrical properties of ZnO-Bi_2O_3-Co_2O_3 varistor by flash sintering. *J. Mater. Sci.-Mater. Electron.* **2022**, *33*, 17900–17911. [CrossRef]
2. Apaydin, F.; Celik, A.; Kara, F.; Toplan, H.O. Comparison of electrical properties of ZnO-Bi_2O_3-based ceramics prepared by conventional and spark plasma sintering (SPS) methods. *J. Aust. Ceram. Soc.* **2022**, *58*, 831–839. [CrossRef]
3. Shi, M.; Zhang, L.; Cheng, Z.; Wang, Z.; He, Q.; Qin, J.; Jiu, Y.; Tang, B.; Xu, D. Effect of La_2O_3 doping on microstructure and electrical properties of flash-sintered ZnO-Bi_2O_3 varistor. *J. Mater. Sci.-Mater. Electron.* **2022**, *33*, 23437–23446. [CrossRef]
4. Peiteado, M. Zinc oxide-based ceramic varistors. *Bol. Soc. Esp. Ceram. Vidr.* **2005**, *44*, 77–87. [CrossRef]
5. Takada, M.; Sato, Y.; Yoshikado, S.; Levinson, L. Relation between Grain Boundary Structure and Electrical Degradation in Zinc Oxide Varistors. *J. Am. Ceram. Soc.* **2012**, *95*, 2579–2586. [CrossRef]
6. Wang, Y.; Peng, Z.; Wang, Q.; Fu, X. Highly nonlinear varistors from oxygen-deficient zinc oxide thin films by hot-dipping in Bi_2O_3: Influence of temperature. *Appl. Surf. Sci.* **2016**, *390*, 92–99. [CrossRef]
7. Wang, Y.; Qi, H.; Wang, Q.; Peng, Z.; Fu, X. Effect of thermal treatment time on high-performance varistors prepared by hot-dipping oxygen-deficient zinc oxide thin films in bismuth oxide powder. *J. Mater. Sci. Mater. Electron.* **2018**, *29*, 20885–20894. [CrossRef]
8. Nie, Y.; Xie, Y.; Zheng, Y.; Luo, Y.; Zhang, J.; Yi, Z.; Zheng, F.; Liu, L.; Chen, X.; Cai, P.; et al. Preparation of ZnO/Bi_2O_3 Composites as Heterogeneous Thin Film Materials with High Photoelectric Performance on FTO Base. *Coatings* **2021**, *11*, 1140. [CrossRef]
9. Medina, J.C.; Portillo-Vélez, N.S.; Bizarro, M.; Hernández-Gordillo, A.; Rodil, S.E. Synergistic effect of supported ZnO/Bi_2O_3 heterojunctions for photocatalysis under visible light. *Dye. Pigment.* **2018**, *153*, 106–116. [CrossRef]
10. Carcia, P.F.; McLean, R.S.; Reilly, M.H.; Nunes, G. Transparent ZnO thin-film transistor fabricated by rf magnetron sputtering. *Appl. Phys. Lett.* **2003**, *82*, 1117–1119. [CrossRef]
11. Kluth, O.; Schöpe, G.; Rech, B.; Menner, R.; Oertel, M.; Orgassa, K.; Werner Schock, H. Comparative material study on RF and DC magnetron sputtered ZnO:Al films. *Thin Solid Film.* **2006**, *502*, 311–316. [CrossRef]
12. Ji, Z.G.; Huang, D.; Xi, J.H.; Ke, W.Q.; Zou, R.F. Ultra-Low-Threshold Varistors Based on Columnar ZnO Thin Films. *J. Mater. Sci. Eng.* **2009**, *27*, 9–11.
13. Kashuba, A.; Ilchuk, H.; Petrus, R.; Semkiv, I.; Bovgyra, O.; Kovalenko, M.; Dzikovskyi, V. Optical properties of Al-doped ZnO thin films obtained by the method of high-frequency magnetron sputtering. *Mod. Phys. Lett. B* **2021**, *35*, 2150189. [CrossRef]

14. Chen, X.-L.; Wang, F.; Geng, X.-H.; Huang, Q.; Zhao, Y.; Zhang, X.-D. Natively textured surface hydrogenated gallium-doped zinc oxide transparent conductive thin films with buffer layers for solar cells. *Thin Solid Film.* **2013**, *542*, 343–347. [CrossRef]
15. Herrera, V.; Díaz-Becerril, T.; Reyes-Cervantes, E.; García-Salgado, G.; Galeazzi, R.; Morales, C.; Rosendo, E.; Coyopol, A.; Romano, R.; Nieto-Caballero, F. Highly Visible Photoluminescence from Ta-Doped Structures of ZnO Films Grown by HFCVD. *Crystals* **2018**, *8*, 395. [CrossRef]
16. Singh, S.K.; Hazra, P.; Tripathi, S.; Chakrabarti, P. Optical characterization of Mg-doped ZnO thin films deposited by RF magnetron sputtering technique. *AIP Conf. Proc.* **2016**, *1728*, 020168.
17. Lu, J.J.; Lu, Y.M.; Tasi, S.I.; Hsiung, T.L.; Wang, H.P.; Jang, L.Y. Conductivity enhancement and semiconductor–metal transition in Ti-doped ZnO films. *Opt. Mater.* **2007**, *29*, 1548–1552. [CrossRef]
18. Chen, Z.; Li, F.; Chen, X.; Xu, S.; Xiong, D.; Huang, Y.; Deng, W. Influence of sintering temperatures of ceramic targets on microstructures and photoelectric properties of titanium-doped ZnO nano-films. *J. Mater. Sci. Mater. Electron.* **2016**, *28*, 4654–4660. [CrossRef]
19. Chitrada, K.C.; Raja, K.S. Nanoporous anodic bismuth oxide for electrochemical energy storage. *ECS Trans.* **2014**, *61*, 55. [CrossRef]
20. Gomez, C.L.; Depablos-Rivera, O.; Medina, J.C.; Silva-Bermudez, P.; Muhl, S.; Zeinert, A.; Rodil, S.E. Stabilization of the delta-phase in Bi_2O_3 thin films. *Solid State Ion.* **2014**, *255*, 147–152. [CrossRef]
21. Saji, K.J.; Populoh, S.; Tiwari, A.N.; Romanyuk, Y.E. Design of p-CuO/n-ZnO heterojunctions by rf magnetron sputtering. *Phys. Status Solidi* **2013**, *210*, 1386–1391. [CrossRef]
22. Liu, Y.; Zhu, S. Preparation and characterization of Mg, Al and Ga co-doped ZnO transparent conductive films deposited by magnetron sputtering. *Results Phys.* **2019**, *14*, 102514. [CrossRef]
23. Chen, H.; Ma, S.; Li, Y.; Ma, L.; Huang, X. Microstructures and optical absorption of Ti-doped ZnO films. In Proceedings of the 2011 International Conference on Electronics, Communications and Control (ICECC), Ningbo, China, 9–11 September 2011; pp. 906–909.
24. Chen, H.; Ding, J.; Shi, F.; Li, Y.; Guo, W. Optical properties of Ti-doped ZnO films synthesized via magnetron sputtering. *J. Alloys Compd.* **2012**, *534*, 59–63. [CrossRef]
25. Lunca Popa, P.; Sønderby, S.; Kerdsongpanya, S.; Lu, J.; Bonanos, N.; Eklund, P. Highly oriented δ-Bi_2O_3 thin films stable at room temperature synthesized by reactive magnetron sputtering. *J. Appl. Phys.* **2013**, *113*, 046101. [CrossRef]
26. Vachhani, P.; Rawal, A.H.; Bhatnagar, A.; Rajput, P.; Jha, S.; Bhattacharyya. Absence of ferromagnetism in transition metal (Co, Ni and Cu) doped ZnO films. *Mater. Res. Express* **2019**, *6*, 066103. [CrossRef]
27. Lu, Y.; Huang, J.; Li, B.; Tang, K.; Ma, Y.; Cao, M.; Wang, L.; Wang, L. A boron and gallium co-doped ZnO intermediate layer for ZnO/Si heterojunction diodes. *Appl. Surf. Sci.* **2018**, *428*, 61–65. [CrossRef]
28. Morasch, J.; Li, S.; Brötz, J.; Jaegermann, W.; Klein, A. Reactively magnetron sputtered Bi_2O_3 thin films: Analysis of structure, optoelectronic, interface, and photovoltaic properties. *Phys. Status Solidi (A)* **2014**, *211*, 93–100. [CrossRef]

Disclaimer/Publisher's Note: The statements, opinions and data contained in all publications are solely those of the individual author(s) and contributor(s) and not of MDPI and/or the editor(s). MDPI and/or the editor(s) disclaim responsibility for any injury to people or property resulting from any ideas, methods, instructions or products referred to in the content.